Heliyon 10 (2024) e28430

Contents lists available at ScienceDirect

Heliyon

journal homepage: www.cell.com/heliyon

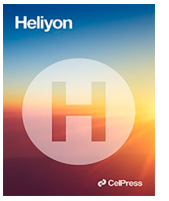

Research article

Nanometals incorporation into active and biodegradable chitosan films

Simona Dordevic [a,*], Dani Dordevic [a], Karolina Tesikova [a], Petr Sedlacek [b], Michal Kalina [b], Lukas Vapenka [c], Marcela Nejezchlebova [d], Jakub Treml [d], Bohuslava Tremlova [a], Hana Koudelková Mikulášková [a]

[a] Department of Plant Origin Food Sciences, Faculty of Veterinary Hygiene and Ecology, University of Veterinary Sciences Brno, Palackeho tr. 1946/1, 612 42, Brno, Czech Republic
[b] Faculty of Chemistry, Brno University of Technology, Purkynova 118, 612 00, Brno, Czech Republic
[c] Department of Food Preservation, University of Chemistry and Technology Prague, Technicka 5, 166 28 Prague 6, Czech Republic
[d] Department of Molecular Pharmacy, Faculty of Pharmacy, Masaryk University, Palackeho tr. 1946/1, 612 00, Brno, Czech Republic

ARTICLE INFO

Keywords:
Packaging
Nanoparticles
Chemical and physical characterization

ABSTRACT

This study investigates the effects of incorporating ZnO, TiO2, and colloidal Ag nanoparticles on the antioxidant, antimicrobial, and physical properties of biodegradable chitosan films. The research focuses on addressing the growing demand for sustainable packaging solutions that offer efficient food preservation while mitigating environmental concerns. In this investigation, the physical properties including thickness, water content, solubility, swelling degree, tensile strength, and elasticity of the chitosan films were examined. Additionally, the samples were analyzed for total polyphenol content, antimicrobial activity, and antioxidant capacity. Notably, the incorporation of ZnO nanoparticles led to the lowest water content and highest strength values among the tested films. Conversely, the addition of colloidal Ag nanoparticles resulted in films with the highest antioxidant capacities (DPPH: 32.202 ± 1.631 %). Remarkably, antimicrobial tests revealed enhanced activity with the inclusion of colloidal silver nanoparticles, yet the most potent antimicrobial properties were observed in films containing ZnO (E.coli: 2.0 ± 0.0 mm; MRSA: 2.0 ± 0.5 mm). The findings of this study hold significant implications for the advancement of edible biodegradable films, offering potential for more efficient food packaging solutions that address environmental sustainability concerns. By elucidating the effects of nanoparticle incorporation on film properties, this research contributes to the ongoing discourse surrounding sustainable packaging solutions in the food industry.

1. Introduction

In recent years, much attention has been focused on edible films as a substitute for petroleum-based materials due to their degradability, sustainability, as well as eco-friendly and non-toxic properties [1,2]. Chitosan is a linear polysaccharide with an amino

* Corresponding author.
E-mail addresses: dordevics@vfu.cz (S. Dordevic), dordevicd@vfu.cz (D. Dordevic), tesikovak@vfu.cz (K. Tesikova), sedlacek-p@fch.vut.cz (P. Sedlacek), kalina-m@fch.vut.cz (M. Kalina), lukas.vapenka@vscht.cz (L. Vapenka), nejezchlebovam@pharm.muni.cz (M. Nejezchlebova), tremlj@pharm.muni.cz (J. Treml), tremlovab@vfu.cz (B. Tremlova), koudelkovamih@vfu.cz (H. Koudelková Mikulášková).

https://doi.org/10.1016/j.heliyon.2024.e28430
Received 8 January 2024; Received in revised form 19 March 2024; Accepted 19 March 2024
Available online 26 March 2024

group and a hydroxyl group, which is widely used in the food industry [3]. It is obtained by deacetylation of chitin, which is abundant in crustaceans. This biopolymer is biodegradable, non-toxic, stable, flexible and has excellent film-forming capabilities. Its antimicrobial and antioxidant properties have made it a suitable alternative for the production of active biodegradable packaging films [4]. Since oxidation is a major food safety issue, a number of packaging systems have been developed containing various antioxidants. Among various antioxidant ingredients, metal nanoparticles represent an auspicious candidate.

Due to their unique properties, nanoparticles are used in many areas such as optics, chemistry, electronics, medicine, etc. They are also used in the food industry in the production, processing, storage and distribution of food [5]. Nanoparticles are added to food packaging to sterilize the food and increase the stability of the packaging [6]. The polymer composites of the packaging are usually mixed in a certain ratio with the metal nanoparticles in the form of an oxide. The particle size of the nano material is in the range of 1–100 nm [7].

ZnO nanoparticles are one of the best-known nanomaterials. ZnO is generally recognised as safe (GRAS) by the FDA. The study conducted by Aristizabal-Gil et al. [8] stated that the combination of nano ZnO and alginate plays an important role in food preservation. The recent works have been indicating the beneficial role of zinc. Bahrampour et al. [9] describe the addition of ZnO nanoparticles to feed as beneficial for improving the quality and quantity of broiler chickens; since zinc is an essential trace element in the body and is involved in a number of enzymatic activities in protein and nucleic acid synthesis [10]. Zinc in the form of nanoparticles is considered as non-toxic to healthy cells, but it is active against cancer cells [11]. The nanoparticle size of ZnO enhances zinc absorption [12] and nutrient absorption in the intestine [13]. Nano ZnO is also characterized by higher antioxidant activity compared to other forms of zinc [14]. ZnO nanoparticles are mainly used as an antibacterial and antifungal agent. A wide range of bacteria are sensitive to ZnO nanoparticles [15].

Zinc oxide nanoparticles exhibit strong antimicrobial activity against a wide range of microorganisms, including bacteria, fungi, and viruses. This property is particularly beneficial for food packaging applications as it helps inhibit the growth of spoilage microorganisms and pathogens, thereby extending the shelf life of packaged foods and reducing the risk of foodborne illnesses [16,17].

The presence of TiO_2 nanoparticles in the packaging protects food against UV radiation [18] and improves the chemical, mechanical and barrier properties of films [19]. The study conducted by Siripatrawan and Kaewklin [20] found that TiO_2 is an oxygen and ethylene scavenger due to photodegradation of ethylene when exposed to sunlight. TiO_2 also shows antimicrobial activity [21]. Though, since 2021, TiO_2 is not considered a safe additive when ingested, however, TiO_2 nanoparticles are permitted in the food industry [22].

Silver is a broad-spectrum antibacterial agent and is currently one of the most commonly used antibacterial agents [23]. Ag nanoparticles have been found to exhibit antioxidant, antimicrobial and anticancer activities [24]. In addition to their antimicrobial properties, silver nanoparticles can also act as an ethylene blocker by being able to absorb and degrade it [25].

The aim of the research was to evaluate the physical characteristics, antioxidant capacity, and antimicrobial activity of biodegradable chitosan films modified with ZnO, TiO2, and colloidal Ag nanoparticles. The study aimed to deepen our understanding of the potential of these modified films as environmentally friendly packaging materials, offering improved food preservation while minimizing environmental impact.

2. Material and methodology

Low-molecular-weight chitosan and ZnO (NPZnO) and TiO_2 ($NPTiO_2$) nanoparticles, as well as other chemicals needed to perform the analyses, were purchased from Sigma-Aldrich (St. Louis, MO, USA). Colloidal silver nanoparticles (NPAg) were purchased from the Koloidni stribro s.r.o. in certified quality.

2.1. Preparation of edible packaging

2.1.1. Production of packaging with the addition of NPZnO, $NPTiO_2$

First, the appropriate nanoparticles (NPZnO or $NPTiO_2$) were weighed out at concentrations of 0.02, 0.2 and 0.5%. Then, 135 ml of 1% lactic acid dissolved in distilled water was added. Subsequently, 1.5 g of chitosan was added and the mixture was stirred. Next, the beaker with the mixture was heated on a hot plate and then stirred using a magnetic stirrer (15 min) at 50 °C and 750 rpm. In the next

Table 1
Composition of prepared edible packaging.

Sample	Composition
CH_L	Chitosan +1% lactic acid + glycerol
$CH_{LZn0,05}$	Chitosan +1% lactic acid +0.05% NPZnO + glycerol
$CH_{LZn0,02}$	Chitosan +1% lactic acid +0.2% NPZnO + glycerol
$CH_{LZn0,5}$	Chitosan +1% lactic acid +0.5% NPZnO + glycerol
$CH_{LTi0,05}$	Chitosan +1% lactic acid +0.05% $NPTiO_2$ + glycerol
$CH_{LTi0,2}$	Chitosan +1% lactic acid +0.2% $NPTiO_2$ + glycerol
$CH_{LTi0,5}$	Chitosan +1% lactic acid +0.5% $NPTiO_2$ + glycerol
CH_{LAg10}	Chitosan +1% lactic acid + colloidal NPAg 10 ppm + glycerol
CH_{LAg30}	Chitosan +1% lactic acid + colloidal NPAg 30 ppm + glycerol
CH_{LAg50}	Chitosan +1% lactic acid + colloidal NPAg 50 ppm + glycerol

step, 0.75 ml of glycerol was added, followed by stirring for 5 min under the same conditions. The film-forming solution was then poured into a 150 cm diameter Petri dish and left to dry for 48 h. The composition of the packaging samples is given in Table 1.

2.1.2. Production of packaging with the addition of NPAg

First, 1.5 g of chitosan was weighed out. Then, 135 ml of 1% lactic acid containing colloidal NPAg at concentrations of 10, 30 and 50 ppm was added and the mixture was stirred. Next, it was heated on a hot plate until liquid and then stirred for 15 min using a magnetic stirrer at 50 °C and 750 rpm. In the next step, 0.75 ml of glycerol was added, after which it was stirred for 5 min and poured into 150 cm diameter Petri dishes and left to dry for 48 h. The composition of the packaging samples is given in Table 1.

Prior to the film formation by their pouring and drying, all the film-forming dispersions were characterized using the method of electrophoretic light scattering with Zetasizer Nano ZS (Malvern Pananalytical). For the analysis, the individual solutions were transferred into spectrometric glass cuvettes (1 cm optical length) containing measuring dip cell (ZEN1002) for zeta potential measurements. The determined values of zeta potential by this technique provide important characteristics of charge present at the polymer chains in film-forming solutions and they can also provide insights into the potential interactions in the system as well as the electrokinetic stability of film-forming solutions.

2.2. Basic characterization of the films

2.2.1. Packaging thickness

The thickness of the dry films was measured using a Mitotuyo M310-25 μm (Kawasaki, Japan). Each measurement was repeated 5 times for each type of packaging.

2.2.2. Water content, solubility and swelling degree

Water content, degree of wetting and solubility were determined according to Souza et al. [26] with minor modifications. For analysis, 3 squares of each package were first cut out (2 × 2 cm), weighed (W1), transferred to weighed dishes and placed in a drying oven (Ecocell 55) at 105 °C for 2 h. The packages were then reweighed (W2) and immersed in beakers with 25 ml of distilled water for 24 h. After 24 h, undissolved samples were reweighed (W3) and placed in a drying oven at 105 °C for 24 h and then reweighed (W4) again.

Water content, degree of wetting and solubility were determined according to the following formulas:

$$\text{Water content } (\%) = [(W - W2)/W1)] \times 100$$

$$\text{Solubility } (\%) = [(W2 - W4)/W2] \times 100$$

$$\text{Swelling degree } (\%) = [(W3 - W2)/W2] \times 100$$

2.3. Structural, morphological and textural analyses of the films

Fourier transform infrared (FTIR) spectra of the films were measured with iS50 FTIR spectrometer (Thermo Scientific, Waltham, MA, USA). All measurements were taken from a surface of a film at ambient temperature (in an air-conditioned room) with the built-in single-reflection diamond attenuated total reflectance (ATR) crystal. First, samples were analyzed in the standard mid-infrared spectral region (4000–400 cm^{-1}). An individual absorption spectrum was collected as an average of 16 scans with a resolution of 4 cm^{-1} (data spacing 0.5 cm–1). Each film was analyzed at 6 randomly distributed spots on both sides of its surface (because of the apparent heterogeneity of its surface, sample $CH_{LZn0.5}$ was alayzed at 10 spots). FTIR spectra, represent an average of the six spectra collected for an individual sample. The whole-spectra PCA analysis was performed in the range of frequencies 1800–800 cm^{-1} using a standard multivariate principle component program written in-house using MATLAB software (MathWorks, Natick, MA, USA) at Institute of Scientific Instruments, Czech Academy of Sciences [27]. Furthermore, the samples were analyzed also in the Far-infrared region (1000–200 cm^{-1}) using the same spectrometer equipped with Solid Substrate beamsplitter. Spectrum was recorded on a single spot of the respective film as an average of 128 scans with the same resolution as in the Mid-infrared region.

Micrographs of all prepared films were recorded using a Zeiss EVO LS-10 scanning electron microscope (SEM) (Carl Zeiss Ltd., Cambridge, UK). Prior to the SEM analysis, a small cut-off of each sample (ca 10 10 mm^2) was stuck on a carbon tape and sputter-coated with gold.

Strength (MPa) and elasticity (%) were measured with a TA.XT plus texture analyser (Godalming, UK), using the ASTM international test method – ASTM D882-02. The produced packages were cut into 1 × 5 cm rectangles and each measurement was performed 5 times.

Water vapour transmission rate (WVTR) was determined by gravimetrical dish method according to DIN 53 122 standard at 23 °C and relative humidity of 85%. Five parallel samples were tested for each packaging material.

Equal pressure method according to ASTM D3985 - 17 standard was used for determination of oxygen permeability by instrument OxTran 2/20 MH (MOCON Inc., USA). Permeability was measured at 23 °C and dry conditions relative humidity of 0%. Two parallel samples were tested for each packaging film.

2.4. Antioxidant activity assays

2.4.1. Total polyphenol content

The total polyphenol content was measured using the Folin-Ciocalteu method according to Tomadoni et al. [28]. 0.1 g of the sample was weighed out into a dark glass vial and then 20 ml of ethanol-water mixture (1:1) was added. Samples were extracted in an ultrasonic bath for 30 min and then 1 ml was collected in a 25 ml volumetric flask; 5 ml of Folin Ciocalteu solution (diluted at 1:10) and 4 ml of 7.5% Na_2CO_3 were added to the sample. The samples were incubated in the dark for 30 min. The absorbance was measured at 765 nm against a blind sample (1 ml of sample was replaced by 1 ml of distilled water). The results were expressed as mg of gallic acid per gram of sample.

2.4.2. FRAP (ferric reducing antioxidant power)

In order to determine the antioxidant activity by the FRAP method according to Behbahani et al. [29], 0.1 g of sample was weighed out, 20 ml of ethanol-water mixture (1:1) was added, and the samples were then sonicated in a water bath for 30 min. Subsequently, 180 μl of the extract was pipetted into dark glass vials, to which 300 μl of distilled water and 3.6 ml of working solution (vinegar buffer, TPTZ and $FeCl_3$) were added. The samples were further incubated in the dark for 8 min. The absorbance was measured at 593 nm against a blind sample (distilled water + working solution). Trolox was used to prepare the calibration curve and the results were expressed as μmol of Trolox per gram of sample.

2.4.3. DPPH (1,1-Diphenyl-2-picrylhydrazyl)

The antioxidant activity was determined by the DPPH method according to Sivarooban et al. [30]. 0.1 g of sample was weighed out into dark glass vials, 20 ml of ethanol-water mixture (1:1) was added, and the samples were sonicated for 30 min and then filtered. 1 ml of 0.1 mM DPPH solution was mixed with 3 ml of the extract and, after 30 min of incubation in the dark, the absorbance was measured using a CECIL spectrophotometer at 517 nm.

$$\text{DPPH } (\%) = [(Abs_{DPPH}\text{-}Abs_{DPPH})/Abs_{DPPH}] \text{ x } 100$$

2.4.4. ABTS (2,2′-azino-bis(3-ethylbenzothiazoline-6-sulfonic acid))

The ABTS method used to determine the antioxidant activity was performed according to Thaipong et al. [31]. 0.1 g of sample was weighed out into dark glass vials, 20 ml of ethanol-water solution (1:1) was added, and the samples were sonicated for 30 min and then filtered. 12–16 h before the measurement, 10 ml of 0.007 M ABTS solution was mixed with 10 ml of 0.00245 M potassium persulphate solution. The solution was diluted before the actual measurement so that its resulting absorbance at 735 nm would be 0.7. Then, 1980 μl of ABTS solution was mixed with 20 μl of the prepared extract. The samples were incubated for 5 min in the dark and then the absorbance was measured at 735 nm. The results were calculated according to the following formula:

$$\text{ABTS } (\%) = [(Abs_{ABTS}\text{-}Abs_{vzorku})/Abs_{ABTS}] \text{ x } 100$$

2.4.5. CUPRAC (cupric reducing antioxidant capacity)

The CUPRAC method used to determine the antioxidant activity was performed according to Apak et al. [32]. 0.1 g of sample was weighed out into dark glass vials, 20 ml of ethanol-water mixture (1:1) was added, and the samples were sonicated for 30 min and then filtered. 1 ml of 0.01 M Copper (II), 1 ml of 0.0075 M Neocuproin, 1 ml of NH4Ac buffer pH = 7.0, 0.1 ml of ethanol-water (1:1) and 1 ml of the extract were mixed. The samples were then incubated in the dark for 1 h and then the absorbance was measured against a blind sample at 450 nm. Trolox was used to prepare the calibration curve and the results were expressed as μmol of Trolox per gram of sample.

2.5. Antimicrobial properties

For the evaluation of antimicrobial properties of films we have used methodology described by Dordevic et al. [33]. Briefly, Each set of films (CHLZn, CHLTi a CHLAg) was tested on each three microorganisms and each plate contained control disc CHL. The diameter of the film discs was 5 mm. The experiments were repeated three times. The results of this method are expressed as an average of inhibition zones diameter (mm) from which the diameter of film discs was substracted.

Reference strains of microorganisms *Staphylococcus aureus* subsp. aureus (MRSA) CCM 7110, *Escherichia coli* CCM 3954 and Candida albicans CCM 8261 were obtained from the Czech Collection of Microorganisms of the Department of Experimental Biology, Faculty of Science, Masaryk University.

2.6. Statistical analysis

All tables present mean values ± standard deviations, where all analyses were performed three times. Statistical significance of $p < 0.05$ was determined by a one-way ANOVA test using parametric Tukey's test (when Leven's test showed $p > 0.05$) and non-parametric

Games-Howell post hoc test (when Leven's test showed $p < 0.05$). The IBM SPSS software was used for statistical processing.

3. Results and discussion

3.1. Influence of NPs on colloidal stability of film-forming dispersions

Zeta potential indicates the stability of particles against aggregation of particles, if the particles have above +30 mV or under 30 mV the particles are stable. The zeta potential is connected with the surface charge of particles. The samples $CH_{LZn0,05}$ and $CH_{LZn0,2}$ are similar, there is only a small difference in surface chemistry (Table 2). On the contrary in the sample $CH_{LZn0,5}$ there is a significant decrease of zeta potential towards zero leading to destabilization of colloid particles.

In the samples with the addition of $NPTiO_2$ the all particles are positively charged. The sample $CH_{LTi0,5}$ is stable, with the higher concentration of $NPTiO_2$ the stability against aggregation is lower (zeta potential towards zero). The all samples with NPAg have positive surface zeta potential and are stable against aggregation of particles.

3.2. Effect of NPs on the basic physico-chemical and textural characteristics of the films

Table 3 shows the results of film thickness measurements. The thickness of the films ranges from 0.182 to 0.232 mm. No statistically significant difference was observed between the films ($p < 0.05$).

Compared to the CH_L sample, the addition of NPZnO increased the film thickness in most samples. The highest value was observed in the sample with NPZnO concentration of 0.2%. The increase in thickness could be due to the presence of solids [34].

Compared to the CH_L sample, similar or lower thickness values were observed in samples with the addition of $NPTiO_2$. Although the addition of NPTiO2 can, according to the study by Chang et al. [35], increase the film thickness, this was not clearly confirmed in this measurement. This may be due to the good distribution of substances in the matrix, and the individual components may have formed intermolecular interactions [36].

In samples containing colloidal NPAg, the thickness values decreased with increasing concentration; however, compared to the package with chitosan only, there was a higher thickness in most samples. These results are consistent with the results of the study by Ortega et al. [37].The sample with a colloidal NPAg concentration of 10 ppm showed the highest thickness value.

The results of water content, solubility and swelling degree are given in Table 4. The results of the measurements show that as the concentration of NPZnO increases, the water content in the films decreases. The chitosan-only film showed the highest water content, which may be due to the abundance of hydrophilic groups in chitosan molecules, especially –OH and $–NH_2$ [38]. The addition of NPZnO may have affected these interactions by the coordination effect between ZnO nanoparticles and –OH/-NH_2 groups of chitosan [39]. In terms of solubility, the addition of NPZnO caused an increase in values in most samples with the increasing nanoparticle concentration ($p < 0.05$). The result shows that the addition of NPZnO increases the swelling degree with increasing concentration.

After the addition of $NPTiO_2$, the water content in the films changed only slightly or decreased. According to the results, the addition of $NPTiO_2$ caused a decrease in the solubility values, where the lowest solubility value was shown by a sample with a nanoparticle concentration of 0.5%. The decreasing trend of water content and solubility depending on the increasing content of $NPTiO_2$ was also observed in the study by Arezoo et al. [40]. The interaction of hydrogen bonds between the hydroxyl groups on the surface of TiO2 and the film molecules can transfer some of the original hydrogen bond interactions between the packaging matrix and the water molecules, thereby reducing the number of water molecules [41]. The addition of $NPTiO_2$ caused an increase in the swelling degree.

Small changes in water content were also observed in samples with the addition of colloidal NPAg, where the sample with a concentration of 50 ppm showed the highest value. By contrast, the solubility decreased with increasing concentration of nanoparticles. The addition of colloidal NPAg increased the value of the swelling degree.

The results of the texture of the packages expressed as tensile strength and elasticity are given in Table 5. Strong mechanical properties can improve the durability of the material during overall handling and storage [42]. The addition of NPZnO caused an

Table 2
Zeta potential and conductivity of film forming solutions.

Sample	Zeta potential (mV)	Conductivity (mS/cm)
CH_L	40.44 ± 2.66^a	1.86 ± 0.08^a
$CH_{LZn0,05}$	38.91 ± 3.12^a	2.07 ± 0.10^b
$CH_{LZn0,2}$	38.58 ± 3.54^a	2.81 ± 0.20^c
$CH_{LZn0,5}$	13.14 ± 1.91^b	3.09 ± 0.10^d
CH_L	40.44 ± 2.96^a	1.86 ± 0.08^a
$CH_{LTi0,05}$	37.56 ± 3.25^a	1.97 ± 0.09^a
$CH_{LTi0,2}$	13.78 ± 1.91^b	2.15 ± 0.09^b
$CH_{LTi0,5}$	6.23 ± 2.47^c	2.85 ± 0.12^c
CH_L	40.44 ± 2.96^a	1.86 ± 0.08^a
CH_{LAg10}	42.88 ± 1.97	1.70 ± 0.01^{bc}
CH_{LAg30}	43.65 ± 1.87	1.69 ± 0.04^b
CH_{LAg50}	46.55 ± 3.75^b	1.86 ± 0.11^c

* superscripts show statistically significant differences ($p < 0.05$) between rows.

Table 3
Thickness measurement of prepared packaging.

Sample	Thickness (mm)
CH_L	0.212 ± 0.068
$CH_{LZn0,05}$	0.214 ± 0.033
$CH_{LZn0,2}$	0.230 ± 0.051
$CH_{LZn0,5}$	0.226 ± 0.027
CH_L	0.212 ± 0.068
$CH_{LTi0,05}$	0.182 ± 0.019
$CH_{LTi0,2}$	0.212 ± 0.044
$CH_{LTi0,5}$	0.192 ± 0.046
CH_L	0.212 ± 0.068
CH_{LAg10}	0.232 ± 0.013
CH_{LAg30}	0.228 ± 0.037
CH_{LAg50}	0.212 ± 0.015

* superscripts show statistically significant differences ($p < 0.05$) between rows.

Table 4
Results of water content (%), solubility (%) and swelling degree (%) of prepared packaging.

Sample	Water content (%)	Solubility (%)	Swelling degree (%)
CH_L	18.216 ± 0.800^a	47.700 ± 2.43^a	254.394 ± 54.379^a
$CH_{LZn0,05}$	15.365 ± 1.123^{ab}	47.213 ± 0.847^a	332.334 ± 8.853^a
$CH_{LZn0,2}$	14.131 ± 0.776^b	58.864 ± 0.589^b	524.736 ± 21.448^a
$CH_{LZn0,5}$	9.123 ± 0.136^c	69.673 ± 0.585^c	3893.941 ± 646.45^b
CH_L	18.216 ± 0.800^a	47.700 ± 2.43^a	254.394 ± 54.379
$CH_{LTi0,05}$	18.767 ± 0.481^b	36.884 ± 2.123^b	291.715 ± 11.543
$CH_{LTi0,2}$	16.888 ± 0.605^c	36.991 ± 0.138^b	256.372 ± 7.306
$CH_{LTi0,5}$	18.602 ± 1.065^c	31.248 ± 0.855^b	312.391 ± 54.572
CH_L	18.216 ± 0.800	47.700 ± 2.43^a	254.394 ± 54.379
CH_{LAg10}	18.084 ± 1.755	43.184 ± 0.750^a	260.792 ± 8.138
CH_{LAg30}	20.074 ± 1.219	38.237 ± 2.197^b	278.159 ± 35.280
CH_{LAg50}	20.931 ± 1.448	38.075 ± 0.221^b	273.701 ± 8.036

* superscripts (a, b,c) show statistically significant differences ($p < 0.05$) between rows.

increase in the values of tensile strength and, conversely, a decrease in the values of elasticity. Similar results were demonstrated in the study by Sanuja et al. [43], where ZnO-containing packaging showed higher tensile strength values. The sample apparently showed a good distribution of NPZnO particles.

Compared to the CH_L sample, an increase in tensile strength values was observed in most of the packaging containing $NPTiO_2$. The authors of the study, Li et al. [44], reported that $NPTiO_2$ increased the cohesive force, decreased the elasticity and thus increased the tensile strength, which was also confirmed in the elasticity results, where there was a decrease in values due to the addition of $NPTiO_2$. The ability to increase tensile strength and reduce elasticity after the addition of TiO_2 is also mentioned by Dash et al. [45]. The increase in the stiffness of the TiO_2-containing film is related to the fact that TiO_2 acts as an antiplasticizer and its presence in the matrix can improve the compactness of the structure [46].

There was a slight increase in tensile strength when using colloidal NPAg. Increased tensile strength may be related to a stronger bond between NPAg and chitosan through the formation of hydrogen and ester bonds [47]. However, no statistically significant

Table 5
Strength (MPa) and elasticity (%) results of prepared packaging.

Sample	Tensile strength (MPa)	Elasticity (%)
CH_L	0.047 ± 0.026^a	114.415 ± 12.451^a
$CH_{LZn0.05}$	0.121 ± 0.044^{ab}	104.752 ± 10.927^a
$CH_{LZn0.2}$	0.279 ± 0.074^c	88.750 ± 7.376^a
$CH_{LZn0.5}$	0.121 ± 0.044^{bc}	104.752 ± 10.927^b
CH_L	0.047 ± 0.026	114.415 ± 12.451
$CH_{LTi0.05}$	0.048 ± 0.012	104.003 ± 4.885
$CH_{LTi0.2}$	0.061 ± 0.016	111.157 ± 5.106
$CH_{LTi0.5}$	0.079 ± 0.025	104.847 ± 9.219
CH_L	0.047 ± 0.026	114.415 ± 12.451^a
CH_{LAg10}	0.057 ± 0.015	133.422 ± 9.863^a
CH_{LAg30}	0.067 ± 0.022	121.894 ± 9.306^b
CH_{LAg50}	0.053 ± 0.021	125.718 ± 15.505^b

* superscripts show statistically significant differences ($p < 0.05$) between rows in the same column.

difference was confirmed here ($p < 0.05$). As part of the elasticity results, an increase in values was observed compared to the CH_L sample.

3.3. Effect of NPs on the film structure, morphology and barrier properties

Mid-infrared spectra of the samples are shown in Fig. 1. Spectrum of the reference chitosan film without addition of any NPs (CH_L) shows typical signals of the main components (chitosan, lactic acid, glycerol), as it was already described in details in our previous study [33]. As far as an effect of NPs' presence in the films is concerned, it can be seen in Fig. 1 that only a higher addition of ZnO NPs induces a noticeable change in the mid-infrared spectrum of the film. Significant change of the vibration pattern can be observed mainly in the FTIR spectrum of $CH_{LZn0.5}$. This film also showed visible differences in the surface homogeneity compared to another NPs-containing chitosan films. Obviously, this particular composition of the film resulted in a limited compatibility of its chemical components. Sharp narrow vibration bands that can be seen in the spectrum of this sample indicates precipitation of a crystalline low-molecular compound. From a detail interpretation of the spectrum, we propose that the high concentration of ZnO NPs in the film-casting solution induced precipitation of zinc lactate during the film formation. This is indicated not only by disappearance of the characteristic C═O stretching band of carboxylic groups (1728 cm^{-1}) in the spectrum of $CH_{LZn0.5}$. and the increasing signal of $–COO^-$ at 1600 and 1400 cm^{-1}, but also by the characteristic pattern of zinc lactate in the range 1300–1000 cm^{-1}, marked with arrows in Fig. 1 [48]. Formation of higher amounts of zinc lactate induced by ZnO nanoparticles in lactic acid solutions have already been described [48]. Local precipitation of water-soluble zinc lactate in the structure of $CH_{LZn0.5}$ film may also explain the stepwise increase in swelling and solubility of the film, as well as the apparent decrease of the film compactness, represented by the reversal of the trends of tensile strength and elasticity (compared to other films containing ZnO NPs). Obviously, usability of ZnO nanoparticles as an additive into chitosan films prepared using aqueous lactic acid as a solvent is limited as it constrains the compatibility of the components and the phase homogeneity of the resulting films.

Characteristic infrared signatures of inorganic nanoparticles appear in the spectral region bellow 1000 cm^{-1}. Therefore, we further approached this respective region implementing the Far-FTIR analysis. Far-infrared spectra of the prepared chitosan films are shown in Fig. 2. As expected, no characteristic vibration bands were observed for Ag nanoparticles (Fig. 2a) because of the absence of any vibrating chemical bonds in the structure of the particles. On the other hand, strong characteristic pattern of Zn–O vibration can be found in spectra of ZnO NPs-containing films (marked with arrows in Fig. 2c) [49,50]. Compared to ZnO NPs, presence of TiO_2 nanoparticles apparently does not result in such significant change in the Far-infrared spectrum, nevertheless, an obvious increase in absorbance in the wide range of 700–400 cm^{-1} can be seen in Fig. 2b for the TiO_2-containing films, which was repeatedly assigned in literature to the Ti–O vibration in anatase [51,52].

Apart from the Far-infrared analysis, that was used to trace the signal of nanoparticles themselves, we have also aimed at evaluation of the interactions between the nanoparticles and the polymer matrix of the film. For this purpose, we applied Principal Component Analysis of the mid-infrared spectra in the region where the most important characteristic vibrations of the organic components of the film occurs (1800–800 cm^{-1}). The principle and the way of presenting and interpreting the results of PCA were explained in our previous study [33]. As it was illustrated in our previous study [33] this approach allows to differentiate spectra with a spectral differences that cannot be identified visually.

Fig. 3a shows the results of PCA analysis of the whole set of prepared samples. Obviously, sample $CH_{LZn0.5}$ is the best distinguished as it clusters away from the other samples. From the loading of the PC1 component, it can be seen that the identified spectral

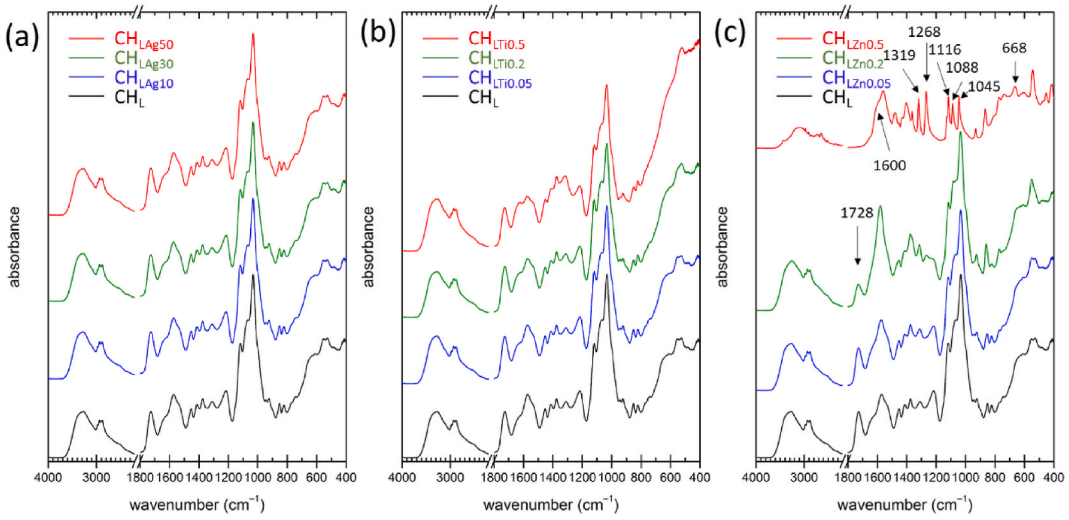

Fig. 1. Mid-infrared spectra of chitosan films prepared without and with addition of (a) AgNPs, (b) TiO_2NPs, and (c) ZnONPs. Every spectrum represents an average of spectra recorded separately on six randomly distributed spots of the film surfaces (three on each side).

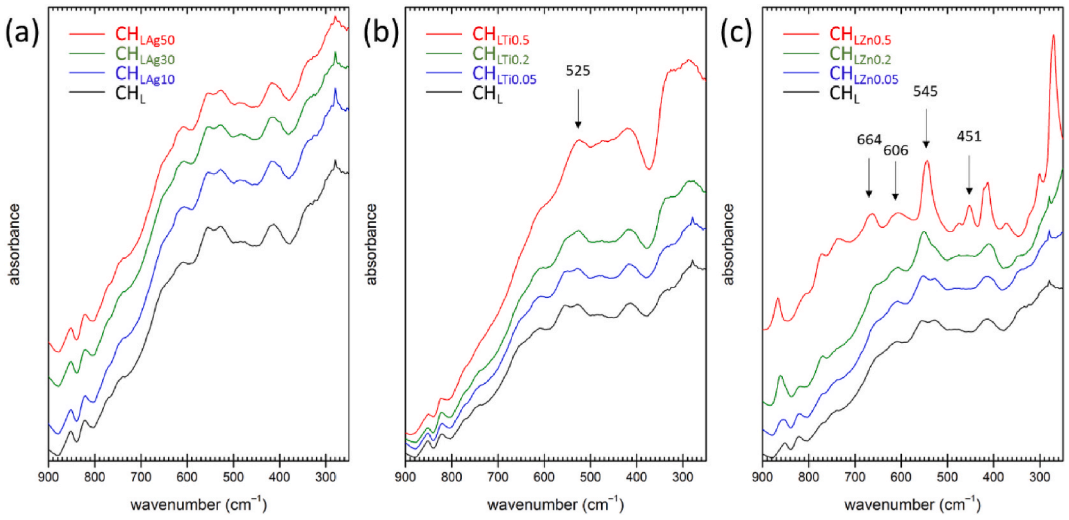

Fig. 2. Far-infrared spectra of chitosan films prepared without and with addition of (a) AgNPs, (b) TiO_2NPs, and (c) ZnONPs.

differences relate mainly to the formation of zinc lactate as discussed above. Not to overweight the other spectral differences by this single deviant sample, we have excluded $CH_{LZn0.5}$ from the further PCA (see Fig. 3b). Results of this analysis shows evident separation of other ZnO NPs-containing films (according to component PC1) as well as the films with an addition of TiO_2 NPs (according to PC2). From the loading of both components, it is obvious that mainly the oxygen- and nitrogen-containing groups of chitosan participate on the interactions with both types of NPs. These includes amide groups (characteristic bands at about 1640 and 1330 cm^{-1}), deacetylated amines (1580 cm^{-1}), glycosidic bonds (1130 cm^{-1}) and hydroxyls (C–O stretching bands at 1000–1100 cm^{-1}). Furthermore, contribution of lactic acid on the interaction with NPs is illustrated by loading of principal components at about 1730 (C═O stretching), and 1210 cm^{-1} (C–O stretching), respectively. These results are consistent with previously published studies on interactions of TiO2 and ZnO NPs with organic matrices [49,53] and they also support the above explanation of the decrease in residual hydration of the films as the result of NPs-chitosan interactions. Fig. 3c shows the results of PCA analysis of the set of samples including reference chitosan film and the films with the addition of Ag NPs. No evident clustering of the samples can be seen, which indicates that interactions between these NPs and chitosan are less pronounced in the FTIR spectra. This is in good agreement with results of the previous study [39], where intermolecular interactions of chitosan-with organic component of the film (purple corn extract) were proved to be much stronger than those of chitosan-AgNPs.

The results of SEM analysis (examples of the results are shown in Figs. 4 and 5) confirmed that the effect of NPs' presence on the morphology of the chitosan films was negligible, with the only exception of the highest content of ZnO NPs. While the surface of this film (sample $CH_{LZn0.5}$) was rough and heterogeneous, the surfaces of all other films were smooth, with randomly located cracks, most probably formed during solvent evaporation, and/or evacuation of the sample before the SEM analysis. Apparently, the cracks are the most pronounced in the reference chitosan film (CH_L) which indicates that the presence of NPs in the structure (especially in the films where the NPs are complexed via the polar groups of the chitosan matrix) may support the compactness of the film, preventing it from a structure collapse caused by dehydration.

Analysis of the barrier properties of the films (Table 6) shows that the increasing content of NPs in general causes a decrease in gas permeability of the chitosan films. For all tested materials, with the exception of the addition of 0.05% ZnO NPs ($CH_{LZn0.5}$), it was statistically proven (ANOVA, $\alpha = 0.05$) that both monitored barrier properties improved after the addition of particles. These results correspond with other results in other publications [54,55]. The improvement of the barrier properties after the addition of nanoparticles is explained by the changes of the structure, mobility of the molecules and formation of local barriers in the structure of the material, while the passing medium goes trough material more difficulty [56,57]. From the point of view of the dependence of the barrier properties on the amount of particles, it can be stated that the higher the particle content means the lower the permeability of the material. This dependence is polynomial and the greatest relative increase in barrier properties compared to the material without the addition of NPs is already achieved with the addition of 0.05% of NPs. The subsequent 4-fold (0.2%) and 10-fold (0.5%) addition of NPs does not improve the barrier properties by as much, which may be due to the fact that the higher content of NPs could also be related to the presence of morphological or structural defects in the materials. Unfortunately, the above evaluation is not possible for WVTR for material with the addition of ZnO NPs. The highest permeability of the reference chitosan films could also be related to the presence of morphological defects such as the cracks shown by the SEM analysis. Nevertheless, it is difficult to judge by how much these defects are caused by an excessive dehydration of the samples during SEM analysis. Furthermore, because the addition of 0.05% ZnO caused, on the contrary, an increase in WVTR (statistically insignificant) and a small decrease in permeability for oxygen. Furthermore, the film with the highest content of ZnO NPs ($CH_{LZn0.5}$) stands alone with the gas permeability below because these materials are not measurable (high fragility with high amount of cracks) by the method used the limit of detection. This unique position of this composition can once again be assigned to the heterogeneity of the film with a significant amount of inorganic crystalline

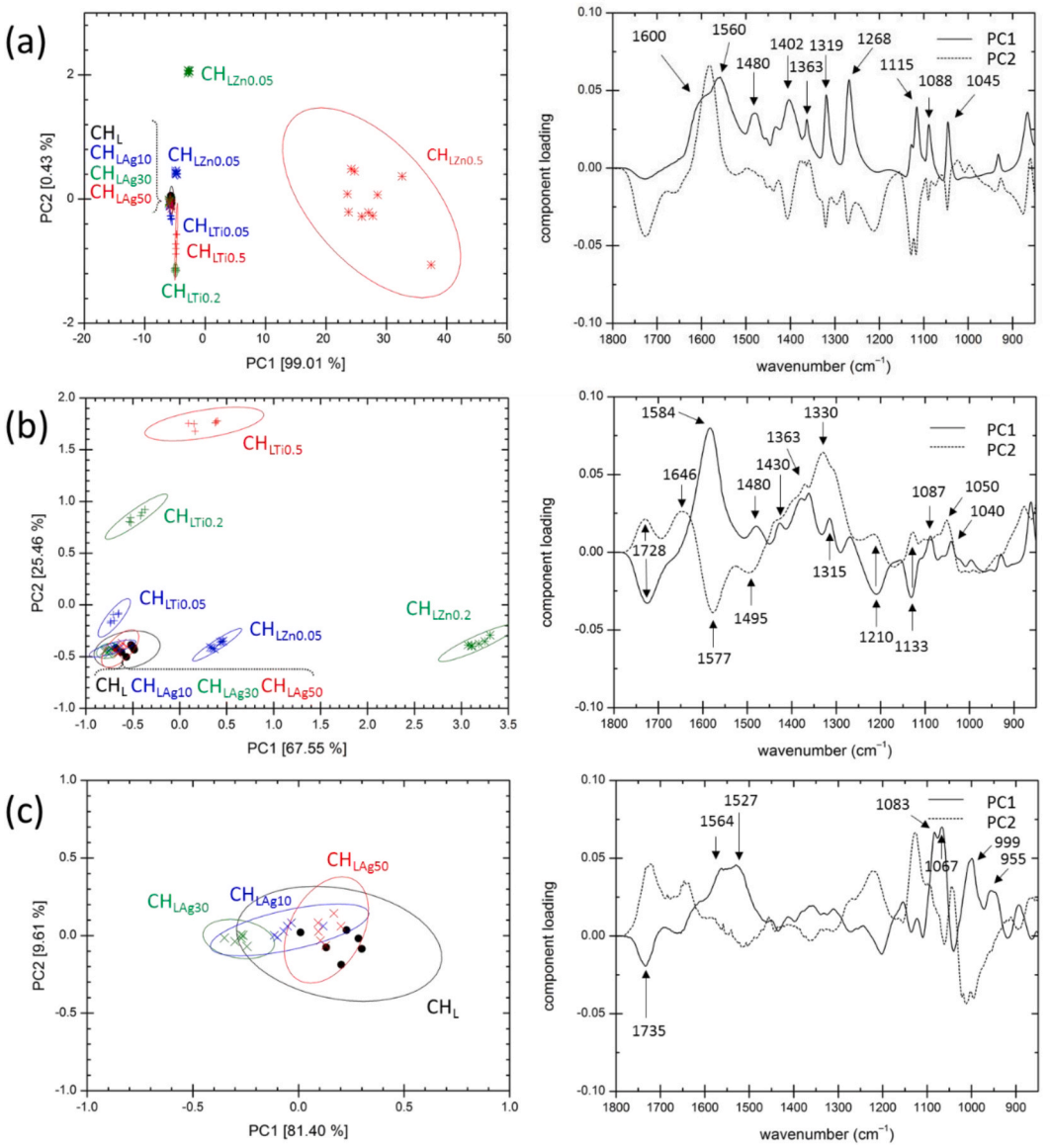

Fig. 3. Results of Principal Component Analyses of the various sets of chitosan films prepared without and with addition of various NPs: (a) the set of all prepared films, (b) the set of all prepared films excluding sample $CH_{LZn0.5}$, (c) the set comprising samples with addition of AgNPs and the reference chitosan film. The PCA was performed with all measured spectra (10 for $CH_{LZn0.5}$, 6 for the other films). The value in the square bracket represents the relative variance that is composed in the respective principal component. Ellipses represent the 95% interval of confidence.

precipitate (zinc lactate) distributed throughout its structure.

3.4. *Effect of NPs on the antioxidant and antimicrobial performance of the films*

In Table 7, which shows the results from the measurement of the antioxidant activity of chitosan films expressed in terms of gallic acid content, a decrease in the values depending on the increasing concentration of NPZnO content is evident. Of the samples containing NPZnO, the sample with the NPZnO concentration of 0.05% showed the highest concentration.

A similar trend was observed in samples containing $NPTiO_2$, however, gallic acid values were higher when $NPTiO_2$ was used, especially in samples with concentrations of 0.05% and 0.2%.

The results show that the addition of colloidal NPAg caused a decrease in polyphenol content in most samples.

Table 8 shows the results of measuring the antioxidant activity of chitosan films using the DPPH method, which indicates the rate of free radical scavenging. The antioxidant nature of chitosan lies in the reaction between the free amino groups of chitosan and free radicals forming stable macromolecular radicals and ammonium groups [58]. The results show that the highest additions of NPZnO

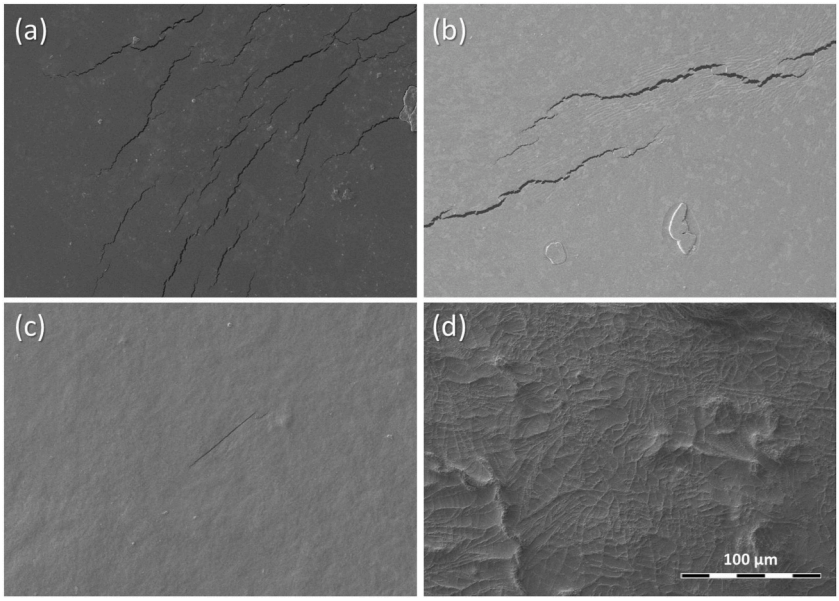

Fig. 4. The SEM micrographs of the surface of (a) CH_L, (b) CH_{LAg50}, (c) $CH_{LTi0.5}$, and (d) $CH_{LZn0.5}$.

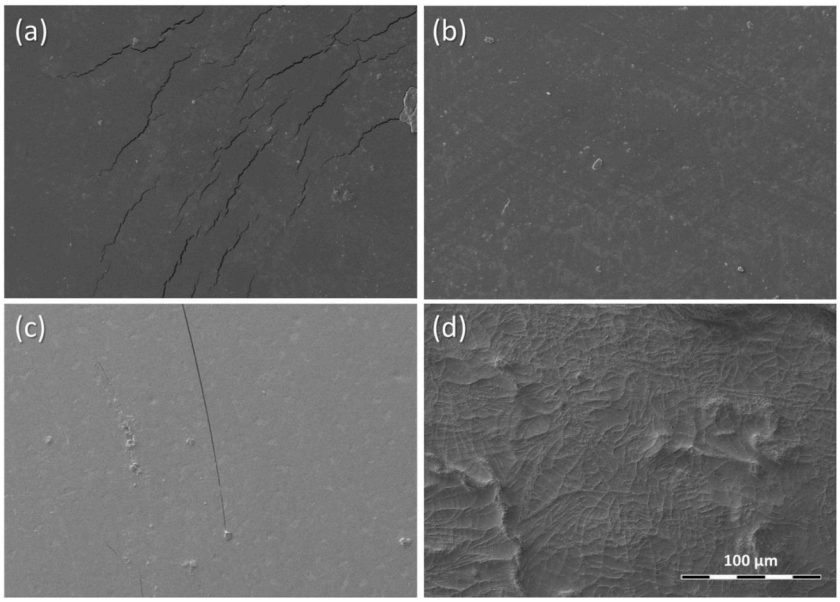

Fig. 5. The SEM micrographs of the surface of (a) CH_L, (b) $CH_{LZn0.05}$, (c) $CH_{LZn0.2}$, and (d) $CH_{LZn0.5}$.

caused a decrease in antioxidant activity. The values of antioxidant activity decrease depending on the increasing concentration of NPZnO. There was a statistically significant difference ($p < 0.05$) between the results containing only NPZnO.

Samples with the addition of $NPTiO_2$ also showed a decrease in antioxidant activities depending on the increasing concentration of $NPTiO_2$. Immobilization of antioxidants on the surface of TiO2 and consequent prevention of free interaction with free radicals can lead to a decrease in values [59].

In the case of films containing colloidal NPAg, the samples showed an increase in antioxidant activities depending on increasing colloid concentration. Colloidal silver is known to have antioxidant properties [7]. The reason could be the ability of silver to donate electrons to free radicals, thereby converting them to a more stable product and terminating the radical chain reaction [1].

The results in Table 8 show the measured values of antioxidant activity using ABTS, which is based on the ability to eliminate free radicals [60]. The results show that NPZnO increased the antioxidant activity of the films. In samples with the addition of NPZnO, the antioxidant activity decreased with increasing concentration of nanoparticles. In case of the packages with NPZnO, the highest

Table 6
Water vapour transmission rate and Oxygen permeability of prepared packaging material.

Sample	Water vapour transmission rate (23 °C, 85 % RH) (g/m^2 d)	Oxygen permeability (23 °C, 0 % RH) (ml/m^2 d 0,1 MPa)
CH_L	1189.1 ± 53.7	14.4 ± 0.5[a]
$CH_{LZn0,05}$	1217.2 ± 97.9[a]	12.3 ± 0.9
$CH_{LZn0,2}$	1078.9 ± 44.2[b]	8.2 ± 0.3[b]
$CH_{LZn0,5}$	N.M.[a]	N.M.[a]
CH_L	1189.1 ± 53.7[a]	14.4 ± 0.5[a]
$CH_{LTi0,05}$	1046.0 ± 34.3[b]	7.7 ± 0.8
$CH_{LTi0,2}$	961.3 ± 34.0[b]	7.2 ± 0.4[b]
$CH_{LTi0,5}$	875.5 ± 17.5[c]	6.2 ± 0.1
CH_L	1189.1 ± 53.7[a]	14.4 ± 0.5[a]
CH_{LAg10}	926.0 ± 29.7[b]	6.2 ± 0.6[b]
CH_{LAg30}	825.5 ± 17.5[c]	5.2 ± 0.0
CH_{LAg50}	754.4 ± 26.2[d]	5.0 ± 0.2[b]

** superscripts show statistically significant differences ($p < 0.05$) between rows.
[a] not measurable.

Table 7
Polyphenol content results (mg gallic acid/mL) of prepared packaging.

Sample	TPC (mg gallic acid/mL)
CH_L	0.957 ± 0.108[a]
$CH_{LZn0,05}$	0.992 ± 0.021[a]
$CH_{LZn0,2}$	0.804 ± 0.038[a]
$CH_{LZn0,5}$	0.358 ± 0.038[b]
CH_L	0.957 ± 0.108[a]
$CH_{LTi0,05}$	1.348 ± 0.080[b]
$CH_{LTi0,2}$	1.338 ± 0.269[b]
$CH_{LTi0,5}$	0.744 ± 0.008[a]
CH_L	0.957 ± 0.108[a]
CH_{LAg10}	0.636 ± 0.045[b]
CH_{LAg30}	1.016 ± 0.029[a]
CH_{LAg50}	0.756 ± 0.010[b]

* superscripts show statistically significant differences ($p < 0.05$) between rows.

Table 8
Antioxidant activity of prepared packaging.

Sample	DPPH (%)	ABTS (%)	FRAP (μmol Trolox/g)	CUPRAC (μmol Trolox/g)
CH_L	17.358 ± 0.901[a]	0.494 ± 0.064[a]	1.849 ± 0.152[a]	9.189 ± 0.424[a]
$CH_{LZn0,05}$	20.395 ± 1.812[b]	1.166 ± 0.043[b]	1.915 ± 0.079[a]	10.088 ± 0.358[b]
$CH_{LZn0,2}$	16.233 ± 1.292[a]	0.875 ± 0.081[c]	1.471 ± 0.144[b]	6.514 ± 0.025[c]
$CH_{LZn0,5}$	12.370 ± 0.298[c]	0.810 ± 0.119[c]	0.821 ± 0.280[c]	1.669 ± 0.071[d]
CH_L	17.358 ± 0.901[a]	0.494 ± 0.064[a]	1.849 ± 0.152	9.189 ± 0.424[a]
$CH_{LTi0,05}$	22.052 ± 1.694[b]	0.279 ± 0.070[b]	1.413 ± 0.144	11.298 ± 0.099[b]
$CH_{LTi0,2}$	20.678 ± 1.573[b]	0.384 ± 0.061[ab]	1.477 ± 0.159	8.562 ± 0.330[c]
$CH_{LTi0,5}$	15.533 ± 1.769[a]	0.404 ± 0.062[ab]	1.223 ± 0.206	4.596 ± 0.218[d]
CH_L	17.358 ± 0.901[a]	0.494 ± 0.064[a]	1.849 ± 0.152[a]	9.189 ± 0.424[a]
CH_{LAg10}	19.502 ± 3.434[ab]	1.781 ± 0.155[b]	1.719 ± 0.029[a]	9.215 ± 0.282[a]
CH_{LAg30}	21.711 ± 2.134[b]	2.145 ± 0.065[c]	2.114 ± 0.202[ab]	9.389 ± 0.306[ab]
CH_{LAg50}	32.202 ± 1.631[c]	2.433 ± 0.101[d]	2.348 ± 0.174[b]	9.999 ± 0.301[b]

* superscripts show statistically significant differences ($p < 0.05$) between rows.

antioxidant activity was observed in the sample with an NPZnO concentration of 0.05% ($p < 0.05$).

Compared to the CH_L sample, samples containing $NPTiO_2$ showed a decrease in antioxidant activities. However, there was a gradual increase in antioxidant activity within individual concentrations.

In the case of addition of colloidal NPAg, the samples showed multiple antioxidant activity compared to the CH_L sample. As the concentration of NPAg increased, the antioxidant activity of the samples increased as well. A statistically significant difference was observed between the individual samples ($p < 0.05$). These results correlate with the results of studies by Otunola and Afolayan [61] and Affes et al. [62].

The results in Table 8 show the measurement of the antioxidant capacity of chitosan films by the FRAP method, which uses the

ability of antioxidants to reduce iron (III > II) [63]. The results with the addition of NPZnO show a decrease in the values of antioxidant capacities depending on the increasing concentration of nanoparticles ($p < 0.05$), however, in comparison with the CH_L sample, a higher activity can be observed in the sample with an NPZnO nanoparticle concentration of 0.05%.

A decrease in antioxidant activity was observed in samples with $NPTiO_2$. The lowest antioxidant activity was observed in the sample with an $NPTiO_2$ concentration of 0.5%, however, no statistically significant difference was confirmed here ($p < 0.05$).

In contrast to the samples containing NPZnO and $NPTiO_2$ nanoparticles, the packaging with the addition of colloidal NPAg showed an increase in antioxidant activity with increasing colloid concentration. This trend is in line with previous results of antioxidant activities.

Table 8 shows the results from the measurement of the antioxidant activity of chitosan films using the CUPRAC method. The addition of NPZnO caused a decrease in the antioxidant activity of the packaging; however, the highest antioxidant activity was shown by the sample with an NPZnO concentration of 0.05%, which is in line with previous results. A statistically significant difference was observed between the samples ($p < 0.05$).

The presence of $NPTiO_2$ caused a decrease in the values of antioxidant activities depending on the increasing concentration of nanoparticles, but compared to the CH_L sample, the sample containing 0.05% $NPTiO_2$ showed a higher antioxidant activity. A statistically significant difference was observed in all samples ($p < 0.05$).

Samples with the addition of colloidal NPAg did not show significant changes in antioxidant activities; however, with increasing concentration of colloidal NPAg, there was also an increase in the antioxidant activity of packaging, which was confirmed in previous results.

ZnO nanoparticles are known for their antibacterial activity. According to Sirelkhatim et al. [64] the mechanism of action is in production of reactive oxygen species (ROS) including hydrogen peroxide and hydroxyl radicals. The production of ROS is followed by damage to cell wall and increased membrane permeability. This is in accordance with results presented in Tables 7 and 8, where the antioxidant capacity of films decreased with increasing concentration of ZnO nanoparticles. The minimal inhibitory concentrations (MIC) of ZnO nanoparticles were determined by Reddy et al. [65] to be 1 mg/ml for *S. aureus* and 3.4 mg/ml for *E. coli*. This agrees with our own results, where the highest concentration used was 5 mg/ml (*i.e.* 0.5%) and we were able to observe an antibacterial effect (Table 9 and Fig. 6).

Nanoparticles containing TiO_2 are also known for their high antibacterial effect as reported by Podporska-Carroll et al. [66]. The tested bacteria were inoculated in growth media containing 50 mg/ml of TiO_2 nanotubes. Growth of *S. aureus* and *E. coli* was reduced after 24 h incubation and UV light exposure Podporska-Carroll et al. [66]. On the other hand, in our experiments we have seen almost no effect, probably due to lower concentration (10 ×) and lack of UV exposure.

Third type of nanoparticles, containing colloidal Ag, was also reported as antibacterial. Kaweeteerawat et al. [67] declared that IC_{50} NPAg were 11.89 mg/l in case of *E. coli* and 6.98 mg/l in case of *S. aureus*. In our experiments, there was almost no effect of NPAg against the tested strains, although the concentration we used was even higher (50 ppm or mg/l). This might be due to some incompatibilities with chitosan films.

4. Conclusion

The escalating environmental concerns associated with petroleum-based packaging materials have necessitated the exploration of alternative solutions, such as the development of environmentally friendly biodegradable edible packaging. In this study, the incorporation of NPZnO, NPTiO2, and colloidal NPAg at various concentrations aimed to enhance the properties of chitosan film. Results indicated that the addition of NPZnO led to a reduction in water content, while simultaneously increasing the values of swelling degree and tensile strength. Conversely, the inclusion of colloidal NPAg improved the elasticity of the packaging, with samples containing it exhibiting notably high antioxidant activity. Additionally, biodegradable films with the incorporation of ZnO nanoparticles demonstrated the highest antimicrobial activity.

By highlighting the potential of incorporating nanoparticles into chitosan film for biodegradable packaging, this research sheds

Table 9
Results of antimicrobial potential testing of prepared packaging.

Sample	Inhibition zones (mm)		
	Escherichia coli	MRSA	*Candida albicans*
CH_L	0.5 ± 0.05	1.0 ± 0.05	0 ± 0.00
$CH_{LZn0,05}$	0.5 ± 0.05	0.5 ± 0.05	not observable inhibition zone
$CH_{LZn0,2}$	2.0 ± 0.05	0.5 ± 0.05	not observable inhibition zone
$CH_{LZn0,5}$	2.0 ± 0.00	2.0 ± 0.05	not observable inhibition zone
CH_L	0.5 ± 0.05	1.0 ± 0.00	0 ± 0.00
$CH_{LTi0,05}$	0.5 ± 0.05	1.0 ± 0.00	0 ± 0.00
$CH_{LTi0,2}$	0.5 ± 0.00	0.5 ± 0.05	0 ± 0.00
$CH_{LTi0,5}$	0.5 ± 0.00	0.5 ± 0.05	0 ± 0.00
CH_L	0.5 ± 0.05	1.0 ± 0.05	0 ± 0.00
CH_{LAg10}	0.5 ± 0.05	1.0 ± 0.00	0 ± 0.00
CH_{LAg30}	1.0 ± 0.05	1.0 ± 0.05	0 ± 0.00
CH_{LAg50}	0.5 ± 0.05	1.0 ± 0.00	0 ± 0.00

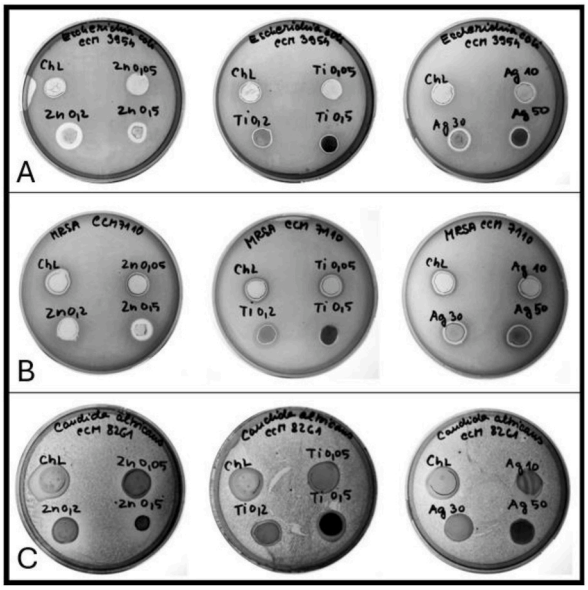

Fig. 6. Photodocumentation of antimicrobial properties of films (A – *Escherichia coli*, B – MRSA, C – *Candida albicans*).

light on the feasibility of mitigating environmental challenges associated with petroleum-based materials. The observed improvements in physical and functional properties, coupled with antimicrobial and antioxidant benefits, underscore the promising applications of these modified films in sustainable packaging solutions. Nevertheless, ongoing exploration and assessment of the packaging's compatibility with food safety standards are imperative to ensure its suitability for commercial adoption.

Data availability statement

All relevant data are within the manuscript.

Ethics declarations

Review and/or approval by an ethics committee was not needed for this study because it is not applicable.

CRediT authorship contribution statement

Simona Dordevic: Writing – review & editing, Writing – original draft, Conceptualization. **Dani Dordevic:** Writing – review & editing, Writing – original draft, Supervision, Methodology, Formal analysis, Conceptualization. **Karolina Tesikova:** Writing – original draft, Formal analysis. **Petr Sedlacek:** Writing – review & editing, Writing – original draft, Visualization, Formal analysis. **Michal Kalina:** Writing – review & editing, Writing – original draft, Formal analysis. **Lukas Vapenka:** Writing – original draft, Formal analysis. **Marcela Nejezchlebova:** Writing – review & editing, Writing – original draft, Formal analysis. **Jakub Treml:** Writing – review & editing, Writing – original draft, Visualization, Formal analysis. **Bohuslava Tremlova:** Writing – original draft, Supervision. **Hana Koudelková Mikulášková:** Writing – original draft, Formal analysis.

Declaration of competing interest

The authors declare that they have no known competing financial interests or personal relationships that could have appeared to influence the work reported in this paper.

Acknowledgements

The research was supported by the University of Veterinary Sciences Brno, grant number 2021ITA24.

References

[1] N. Oladzadabbasabadi, A.M. Nafchi, F. Ariffin, M.J.O. Wijekoon, A.A. Al-Hassan, M.A. Dheyab, M. Ghasemlou, Recent advances in extraction, modification, and application of chitosan in packaging industry, Carbohydr. Polym. 277 (2022) 118876, https://doi.org/10.1016/j.carbpol.2021.118876.

[2] R. Zhao, W. Guan, P. Zheng, F. Tian, Z. Zhang, Z. Sun, L. Cai, Development of edible composite film based on chitosan nanoparticles and their application in packaging of fresh red sea bream fillets, Food Control 132 (2022) 108545, https://doi.org/10.1016/j.foodcont.2021.108545.

[3] H. Wang, J. Qian, H. Li, F. Ding, Rheological characterization and simulation of chitosan-TiO2 edible ink for screen-printing. Progress Org, Coatings 120 (2018) 19–27, https://doi.org/10.1016/j.porgcoat.2018.03.005.

[4] R. Balti, M.B. Mansour, N. Sayari, L. Yacoubi, L. Rabaoui, N. Brodu, A. Massé, Development and characterization of bioactive edible films from spider crab (Maja crispata) chitosan incorporated with Spirulina extract, Int. J. Biol. Macromol. 105 (2017) 1464–1472, https://doi.org/10.1016/j.ijbiomac.2017.07.046.

[5] M. Wang, S. Li, Z. Chen, J. Zhu, W. Hao, G. Jia, W. Chen, Y. Zheng, Q. Weidong, Y. Liu, Safety assessment of nanoparticles in food: current status and prospective, Nano Today 39 (2021) 101169, https://doi.org/10.1016/j.nantod.2021.101169.

[6] O.V. López, L.A. Castillo, M.A. Garcia, M.A. Villar, S.E. Barbosa, Food packaging bags based on thermoplastic corn starch reinforced with talc nanoparticles, Food Hydrocolloids 43 (2015) 18–24, https://doi.org/10.1016/j.foodhyd.2014.04.021.

[7] G. Das, J.K. Patra, T. Debnath, A. Ansari, H.S. Shin, Investigation of antioxidant, antibacterial, antidiabetic, and cytotoxicity potential of silver nanoparticles synthesized using the outer peel extract of Ananas comosus (L.), PLoS One 14 (8) (2019) e0220950, https://doi.org/10.1371/journal.pone.0220950.

[8] M.V. Aristizabal-Gil, S. Santiago-Toro, L.T. Sanchez, M.I. Pinzon, J.A. Gutierrez, C.C. Villa, ZnO and ZnO/CaO nanoparticles in alginate films. Synthesis, mechanical characterization, barrier properties and release kinetics, LWT 112 (2019) 108217, https://doi.org/10.1016/j.lwt.2019.05.115.

[9] K. Bahrampour, N. Ziaei, O.A. Esmaeilipour, Feeding nano particles of vitamin C and zinc oxide: effect on growth performance, immune response, intestinal morphology and blood constituents in heat stressed broiler chickens, Livest. Sci. 253 (2021) 104719, https://doi.org/10.1016/j.livsci.2021.104719.

[10] T.A. Singh, A. Sharma, N. Tejwan, N. Ghosh, J. Das, P.C. Sil, A state of the art review on the synthesis, antibacterial, antioxidant, antidiabetic and tissue regeneration activities of zinc oxide nanoparticles, Adv. Colloid Interfac. 295 (2021) 102495, https://doi.org/10.1016/j.cis.2021.102495.

[11] K.H. Muller, J. Kulkarni, M. Motskin, A. Goode, P. Winship, J.N. Skepper, M.P. Ryan, A.E. Porter, pH-dependent toxicity of high aspect ratio ZnO nanowires in macrophages due to intracellular dissolution, ACS Nano 4 (11) (2010) 6767–6779, https://doi.org/10.1021/nn101192z.

[12] Y.H. Tsai, S.Y. Mao, M.Z. Li, J.T. Huang, T.F. Lien, Effects of nanosize zinc oxide on zinc retention, eggshell quality, immune response and serum parameters of aged laying hens, Anim. Feed Sci. Technol. 213 (2016) 99–107, https://doi.org/10.1016/j.anifeedsci.2016.01.009.

[13] C.Y. Zhao, S.X. Tan, X.Y. Xiao, X.S. Qiu, J.Q. Pan, Z.X. Tang, Effects of dietary zinc oxide nanoparticles on growth performance and antioxidative status in broilers, Biol. Trace Elem. Res. 160 (3) (2014) 361–367, https://doi.org/10.1007/s12011-014-0052-2.

[14] Q. Sun, J. Li, T. Le, Zinc oxide nanoparticle as a novel class of antifungal agents: current advances and future perspectives, J. Agric. Food Chem. 66 (43) (2018) 11209–11220, https://doi.org/10.1021/acs.jafc.8b03210.

[15] V. Zanet, J. Vidic, S. Auger, P. Vizzini, G. Lippe, L. Iacumin, G. Comi, M. Manzano, Activity evaluation of pure and doped zinc oxide nanoparticles against bacterial pathogens and Saccharomyces cerevisiae, J. Appl. Microbiol. 127 (5) (2019) 1391–1402, https://doi.org/10.1111/jam.14407.

[16] K.M. Reddy, K. Feris, J. Bell, D.G. Wingett, C. Hanley, A. Punnoose, Selective toxicity of zinc oxide nanoparticles to prokaryotic and eukaryotic systems, Appl. Phys. Lett. 90 (21) (2007) 213902, https://doi.org/10.1063/1.2742324.

[17] K.R. Raghupathi, R.T. Koodali, A.C. Manna, Size-dependent bacterial growth inhibition and mechanism of antibacterial activity of zinc oxide nanoparticles, Langmuir 27 (7) (2011) 4020–4028, https://doi.org/10.1021/la104825u.

[18] J. Bogdan, A. Jackowska-Tracz, J. Zarzyńska, J. Pławińska-Czarnak, Chances and limitations of nanosized titanium dioxide practical application in view of its physicochemical properties, Nanoscale Res. Lett. 10 (1) (2015) 1–10, https://doi.org/10.1186/s11671-015-0753-2.

[19] L.C. Mohr, A.P. Capelezzo, C.R.D.M. Baretta, M.A.P.M. Martins, M.A. Fiori, J.M.M. Mello, Titanium dioxide nanoparticles applied as ultraviolet radiation blocker in the polylactic acid bidegradable polymer, Polym. Test. 77 (2019) 105867, https://doi.org/10.1016/j.polymertesting.2019.04.014.

[20] U. Siripatrawan, P. Kaewklin, Fabrication and characterization of chitosan-titanium dioxide nanocomposite film as ethylene scavenging and antimicrobial active food packaging, Food Hydrocolloids 84 (2018) 125–134, https://doi.org/10.1016/j.foodhyd.2018.04.049.

[21] M. Mesgari, A.H. Aalami, A. Sahebkar, Antimicrobial activities of chitosan/titanium dioxide composites as a biological nanolayer for food preservation: a review, Int. J. Biol. Macromol. 176 (2021) 530–539, https://doi.org/10.1016/j.ijbiomac.2021.02.099.

[22] M.V. Nikolic, Z.Z. Vasiljevic, S. Auger, J. Vidic, Metal oxide nanoparticles for safe active and intelligent food packaging, Trends Food Sci. Technol. 116 (2021) 655–668, https://doi.org/10.1016/j.tifs.2021.08.019.

[23] N. Lu, Z. Chen, W. Zhang, G. Yang, Q. Liu, R. Böttger, S. Zhou, Y. Liu, Effect of silver ion implantation on antibacterial ability of polyethylene food packing films, Food Packag. Shelf Life 28 (2021) 100650, https://doi.org/10.1016/j.fpsl.2021.100650.

[24] A.K. Biswal, P.K. Misra, Biosynthesis and characterization of silver nanoparticles for prospective application in food packaging and biomedical fields, Mater. Chem. Phys. 250 (2020) 123014, https://doi.org/10.1016/j.matchemphys.2020.123014.

[25] M.A. Emamhadi, M. Sarafraz, M. Akbari, Y. Fakhri, N.T.T. Linh, A.M. Khaneghah, Nanomaterials for food packaging applications: a systematic review, Food Chem. Toxicol. 146 (2020) 111825, https://doi.org/10.1016/j.fct.2020.111825.

[26] V.G.L. Souza, A.L. Fernando, J.R.A. Pires, P.F. Rodrigues, A.A. Lopes, F.M.B. Fernandes, Physical properties of chitosan films incorporated with natural antioxidants, Ind. Crop. Prod. 107 (2017) 565–572, https://doi.org/10.1016/j.indcrop.2017.04.056.

[27] K. Mlynáriková, O. Samek, S. Bernatová, F. Růžička, J. Ježek, A. Hároniková, M. Šiler, P. Zemánek, V. Holá, Influence of culture media on microbial fingerprints using Raman spectroscopy, Sensors 15 (11) (2015) 29635–29647, https://doi.org/10.3390/s151129635.

[28] B. Tomadoni, L. Cassani, A. Ponce, M.D.R. Moreira, M.V. Agüero, Optimization of ultrasound, vanillin and pomegranate extract treatment for shelf-stable unpasteurized strawberry juice, LWT-Food Sci. Technol. 72 (2016) 475–484, https://doi.org/10.1016/j.lwt.2016.05.024.

[29] B.A. Behbahani, F. Shahidi, F.T. Yazdi, S.A. Mortazavi, M. Mohebbi, Use of Plantago major seed mucilage as a novel edible coating incorporated with Anethum graveolens essential oil on shelf life extension of beef in refrigerated storage, Int. J. Biol. Macromol. 94 (2017) 515–526, https://doi.org/10.1016/j.ijbiomac.2016.10.055.

[30] T. Sivarooban, N.S. Hettiarachchy, M.G. Johnson, Physical and antimicrobial properties of grape seed extract, nisin, and EDTA incorporated soy protein edible films, Food Res. Int. 41 (8) (2008) 781–785, https://doi.org/10.1016/j.foodres.2008.04.007.

[31] K. Thaipong, U. Boonprakob, K. Crosby, L. Cisneros-Zevallos, D.H. Byrne, Comparison of ABTS, DPPH, FRAP, and ORAC assays for estimating antioxidant activity from guava fruit extracts, J. Food Compos. Anal. 19 (6–7) (2006) 669–675, https://doi.org/10.1016/j.jfca.2006.01.003.

[32] R. Apak, K. Güçlü, M. Özyürek, S.E. Karademir, Novel total antioxidant capacity index for dietary polyphenols and vitamins C and E, using their cupric ion reducing capability in the presence of neocuproine: CUPRAC method, J. Agric. Food Chem. 52 (26) (2004) 7970–7981, https://doi.org/10.1021/jf048741x.

[33] S. Dordevic, D. Dordevic, P. Sedlacek, M. Kalina, K. Tesikova, B. Antonic, B. Tremlova, J. Treml, M. Nejezchlebova, L. Vapenka, A. Rajchl, M. Bulakova, Incorporation of natural blueberry, red grapes and parsley extract by-products into the production of chitosan edible films, Polymers 13 (19) (2021) 3388, https://doi.org/10.3390/polym13193388.

[34] J. Liu, J. Huang, Z. Hu, G. Li, L. Hu, X. Chen, Y. Hu, Chitosan-based films with antioxidant of bamboo leaves and ZnO nanoparticles for application in active food packaging, Int. J. Biol. Macromol. 189 (2021) 363–369, https://doi.org/10.1016/j.ijbiomac.2021.08.136.

[35] X. Chang, Y. Hou, Q. Liu, Z. Hu, Q. Xie, Y. Shan, L. Gaoyang, S. Ding, Physicochemical and antimicrobial properties of chitosan composite films incorporated with glycerol monolaurate and nano-TiO2, Food Hydrocolloids (2021) 106846, https://doi.org/10.1016/j.foodhyd.2021.106846.

[36] X. Wang, H. Yong, L. Gao, L. Li, M. Jin, J. Liu, Preparation and characterization of antioxidant and pH-sensitive films based on chitosan and black soybean seed coat extract, Food Hydrocolloids 89 (2019) 56–66, https://doi.org/10.1016/j.foodhyd.2018.10.019.

[37] F. Ortega, L. Giannuzzi, V.B. Arce, M.A. García, Active composite starch films containing green synthetized silver nanoparticles, Food Hydrocolloids 70 (2017) 152–162, https://doi.org/10.1016/j.foodhyd.2017.03.036.

[38] H. Liu, R. Adhikari, Q. Guo, B. Adhikari, Preparation and characterization of glycerol plasticized (high-amylose) starch–chitosan films, J. Food Eng. 116 (2) (2013) 588–597, https://doi.org/10.1016/j.jfoodeng.2012.12.037.

[39] Y. Qin, Y. Liu, L. Yuan, H. Yong, J. Liu, Preparation and characterization of antioxidant, antimicrobial and pH-sensitive films based on chitosan, silver nanoparticles and purple corn extract, Food Hydrocolloids 96 (2019) 102–111, https://doi.org/10.1016/j.foodhyd.2019.05.017.

[40] E. Arezoo, E. Mohammadreza, M. Maryam, M.N. Abdorreza, The synergistic effects of cinnamon essential oil and nano TiO2 on antimicrobial and functional properties of sago starch films, Int. J. Biol. Macromol. 157 (2020) 743–751, https://doi.org/10.1016/j.ijbiomac.2019.11.244.
[41] W. Zhang, J.W. Rhim, Titanium dioxide (TiO2) for the manufacture of multifunctional active food packaging films, Food Packag. Shelf Life 31 (2022) 100806, https://doi.org/10.1016/j.fpsl.2021.100806.
[42] L. Ge, M. Zhu, X. Li, Y. Xu, X. Ma, R. Shi, D. Li, C. Mu, Development of active rosmarinic acid-gelatin biodegradable films with antioxidant and long-term antibacterial activities, Food Hydrocolloids 83 (2018) 308–316, https://doi.org/10.1016/j.foodhyd.2018.04.052.
[43] S. Sanuja, A. Agalya, M.J. Umapathy, Synthesis and characterization of zinc oxide–neem oil–chitosan bionanocomposite for food packaging application, Int. J. Biol. Macromol. 74 (2015) 76–84, https://doi.org/10.1016/j.ijbiomac.2014.11.036.
[44] W. Li, K. Zheng, H. Chen, S. Feng, W. Wang, C. Qin, Influence of nano titanium dioxide and clove oil on chitosan–starch film characteristics, Polymers 11 (9) (2019) 1418, https://doi.org/10.3390/polym11091418.
[45] K.K. Dash, N.A. Ali, D. Das, D. Mohanta, Thorough evaluation of sweet potato starch and lemon-waste pectin based-edible films with nano-titania inclusions for food packaging applications, Int. J. Biol. Macromol. 139 (2019) 449–458, https://doi.org/10.1016/j.ijbiomac.2019.07.193.
[46] A.M. Nafchi, S. Mahmud, M. Robal, Antimicrobial, rheological, and physicochemical properties of sago starch films filled with nanorod-rich zinc oxide, J. Food Eng. 113 (4) (2012) 511–519, https://doi.org/10.1016/j.jfoodeng.2012.07.017.
[47] W. Zhang, W. Jiang, Antioxidant and antibacterial chitosan film with tea polyphenols-mediated green synthesis silver nanoparticle via a novel one-pot method, Int. J. Biol. Macromol. 155 (2020) 1252–1261, https://doi.org/10.1016/j.ijbiomac.2019.11.093.
[48] H. Rodríguez-Tobías, G. Morales, F.J. Enríquez-Medrano, D. Grande, Performance of zinc oxide nanoparticles as Polymerization initiating systems in the microwave-assisted synthesis of poly (d, l-Lactide)/ZnO nanocomposites, Macromol. Symp. 374 (2017) 1600102.
[49] S. Hosseini Largani, M. Akbarzadeh Pasha, The effect of concentration ratio and type of functional group on synthesis of CNT–ZnO hybrid nanomaterial by an in situ sol–gel process, Int. Nano Lett. 7 (2017) 25–33, https://doi.org/10.1007/s40089-016-0197-4.
[50] K. Handore, S. Bhavsar, A. Horne, P. Chhattise, K. Mohite, J. Ambekar, N. Pande, V. Chabukswar, Novel green route of synthesis of ZnO nanoparticles by using natural biodegradable polymer and its application as a catalyst for oxidation of aldehydes, J. Macromol. Sci. 51 (12) (2014) 941–947, https://doi.org/10.1080/10601325.2014.967078.
[51] M.M. Ahmad, S. Mushtaq, H.S. Al Qahtani, A. Sedky, M.W. Alam, Investigation of TiO2 nanoparticles synthesized by sol-gel method for effectual photodegradation, oxidation and reduction reaction, Crystals 11 (12) (2021) 1456, https://doi.org/10.3390/cryst11121456.
[52] G. Gohari, A. Mohammadi, A. Akbari, S. Panahirad, M.R. Dadpour, V. Fotopoulos, S. Kimura, Titanium dioxide nanoparticles (TiO2 NPs) promote growth and ameliorate salinity stress effects on essential oil profile and biochemical attributes of Dracocephalum moldavica, Sci. Rep. UK 10 (1) (2020) 912, https://doi.org/10.1038/s41598-020-57794-1.
[53] N.L. Benbow, L. Rozenberga, A.J. McQuillan, M. Krasowska, D.A. Beattie, ATR FTIR study of the interaction of tio2 nanoparticle films with β-Lactoglobulin and bile salts, Langmuir 37 (45) (2021) 13278–13290, https://doi.org/10.1021/acs.langmuir.1c01830.
[54] H. Chi, W. Li, C. Fan, C. Zhang, L. Li, Y. Qin, M. Yuan, Effect of high pressure treatment on poly (lactic acid)/nano–TiO2 composite films, Molecules 23 (10) (2018) 2621, https://doi.org/10.3390/molecules23102621.
[55] A.S.S. Salazar, P.A.S. Cavazos, H.M. Paz, A.V. Fragoso, External factors and nanoparticles effect on water vapor permeability of pectin-based films, J. Food Eng. 245 (2019) 73–79, https://doi.org/10.1016/j.jfoodeng.2018.09.002.
[56] E.H.H. Jamieson, A.H. Windle, Structure and oxygen-barrier properties of metallized polymer film, J. Mater. Sci. 18 (1983) 64–80, https://doi.org/10.1007/BF00543811.
[57] J. Castro-Rosas, A.M. Cruz-Galvez, C.A. Gomez-Aldapa, R.N. Falfan-Cortes, F.A. Guzman-Ortiz, M.L. Rodríguez-Marín, Biopolymer films and the effects of added lipids, nanoparticles and antimicrobials on their mechanical and barrier properties: a review, Int. J. Food Sci. Technol. 51 (2016) 1967–1978, https://doi.org/10.1111/ijfs.13183.
[58] K. Zheng, S. Xiao, W. Li, W. Wang, H. Chen, F. Yang, C. Qin, Chitosan-acorn starch-eugenol edible film: physico-chemical, barrier, antimicrobial, antioxidant and structural properties, Int. J. Biol. Macromol. 135 (2019) 344–352, https://doi.org/10.1016/j.ijbiomac.2019.05.151.
[59] Z. Riahi, R. Priyadarshi, J.W. Rhim, R. Bagheri, Gelatin-based functional films integrated with grapefruit seed extract and TiO2 for active food packaging applications, Food Hydrocolloids 112 (2021) 106314, https://doi.org/10.1016/j.foodhyd.2020.106314.
[60] V. Mareček, A. Mikyška, D. Hampel, P. Čejka, J. Neuwirthová, A. Malachová, R. Cerkal, ABTS and DPPH methods as a tool for studying antioxidant capacity of spring barley and malt, J. Cereal. Sci. 73 (2017) 40–45, https://doi.org/10.1016/j.jcs.2016.11.004.
[61] G.A. Otunola, A.J. Afolayan, In vitro antibacterial, antioxidant and toxicity profile of silver nanoparticles green-synthesized and characterized from aqueous extract of a spice blend formulation, Biotechnol. Biotechnol. Equip. 32 (3) (2018) 724–733, https://doi.org/10.1080/13102818.2018.1448301.
[62] S. Affes, H. Maalej, I. Aranaz, H. Kchaou, N. Acosta, Á. Heras, M. Nasri, Controlled size green synthesis of bioactive silver nanoparticles assisted by chitosan and its derivatives and their application in biofilm preparation, Carbohyd. Polym. 236 (2020) 116063, https://doi.org/10.1016/j.carbpol.2020.116063.
[63] A. Jones, S. Pravadali-Cekic, G.R. Dennis, R. Bashir, P.J. Mahon, R.A. Shalliker, Ferric reducing antioxidant potential (FRAP) of antioxidants using reaction flow chromatography, Anal. Chim. Acta 967 (2017) 93–101, https://doi.org/10.1016/j.aca.2017.02.032.
[64] A. Sirelkhatim, S. Mahmud, A. Seeni, N.H.M. Kaus, L.C. Ann, S.K.M. Bakhori, H. Hasan, D. Mohamad, Review on zinc oxide nanoparticles: antibacterial activity and toxicity mechanism, Nano-Micro Lett. 7 (2015) 219–242, https://doi.org/10.1007/s40820-015-0040-x.
[65] K.M. Reddy, K. Feris, J. Bell, D.G. Wingett, C. Hanley, A. Punnoose, Selective toxicity of zinc oxide nanoparticles to prokaryotic and eukaryotic systems, Appl. Phys. Lett. 90 (21) (2007), https://doi.org/10.1063/1.2742324.
[66] J. Podporska-Carroll, E. Panaitescu, B. Quilty, L. Wang, L. Menon, S.C. Pillai, Antimicrobial properties of highly efficient photocatalytic TiO2 nanotubes, Appl. Catal. B Environ. 176 (2015) 70–75, https://doi.org/10.1016/j.apcatb.2015.03.029.
[67] C. Kaweeteerawat, P. Na Ubol, S. Sangmuang, S. Aueviriyavit, R. Maniratanachote, Mechanisms of antibiotic resistance in bacteria mediated by silver nanoparticles, J. Toxicol. Env. Heal. A. 80 (23–24) (2017) 1276–1289, https://doi.org/10.1080/15287394.2017.1376727.